Geomorphology 278 (2017) 287–297

Contents lists available at ScienceDirect

Geomorphology

journal homepage: www.elsevier.com/locate/geomorph

Geomorphological activity at a rock glacier front detected with a 3D density-based clustering algorithm

Natan Micheletti*, Marj Tonini, Stuart N. Lane

Institute of Earth Surface Dynamics, University of Lausanne, Switzerland

ARTICLE INFO

Article history:
Received 12 July 2016
Received in revised form 30 September 2016
Accepted 18 November 2016
Available online 25 November 2016

Keywords:
Geomorphological activity
Terrestrial laser scanning
Detection of change
Density-based clustering
Rock glacier

ABSTRACT

Acquisition of high density point clouds using terrestrial laser scanners (TLSs) has become commonplace in geomorphic science. The derived point clouds are often interpolated onto regular grids and the grids compared to detect change (i.e. erosion and deposition/advancement movements). This procedure is necessary for some applications (e.g. digital terrain analysis), but it inevitably leads to a certain loss of potentially valuable information contained within the point clouds. In the present study, an alternative methodology for geomorphological analysis and feature detection from point clouds is proposed. It rests on the use of the Density-Based Spatial Clustering of Applications with Noise (DBSCAN), applied to TLS data for a rock glacier front slope in the Swiss Alps. The proposed methods allowed the detection and isolation of movements directly from point clouds which yield to accuracies in the following computation of volumes that depend only on the actual registered distance between points. We demonstrated that these values are more conservative than volumes computed with the traditional DEM comparison. The results are illustrated for the summer of 2015, a season of enhanced geomorphic activity associated with exceptionally high temperatures.

1. Introduction

Terrestrial laser scanning (TLS) has been one of the most successful methods for 3D data collection in the last few years (Alho et al., 2009; Bauer et al., 2003; Deems et al., 2013; Gabbud et al., 2015; Glenn et al., 2006; Heritage and Hetherington, 2007; Schaefer and Inkpen, 2010) and sequential acquisition can be used to detect and quantify surface change (Abellan et al., 2014; Gabbud et al., 2015; Neugirg et al., 2016).

While the development of TLS has made data collection more easily accessible, three challenges arise. First, the large number of points acquired is computationally challenging, and datasets have to be filtered such that only a subset of points is finally retained for the analysis (e.g. Abellan et al., 2006). The consequences of this dataset reduction are dependent on the spatial scales of variability in the surfaces being considered and the questions being asked with those data. It is possible to reduce data density significantly without statistically altering the terrain proprieties at certain (coarser) scales (Chaplot et al., 2001; Gessler et al., 2000). However, representation of more detailed micro-scale topographic characteristics requires a higher density of data points (Anderson et al., 2006; Florinsky and Kuryakova, 2000). If the questions being asked of a dataset relate to change detection (i.e. determination of topographic change, including erosion and deposition), the scale chosen for the analysis will affect the estimations of changes obtained (Lane et al., 1994). Second, terrestrial data collection methods remain important but suffer from perspective effects, which can lead to either zones of occlusion (shadow effect) or spatially-variable point densities. For change detection, such zones need to be treated carefully. Third, in the vast majority of contributions (e.g. Alho et al., 2009; Gabbud et al., 2015; Jaboyedoff et al., 2012) 3D point clouds are interpolated to digital elevation models (DEMs), either as regular raster grids or triangulated irregular networks (TINs). These are effectively 2.5D representations of the topography (Jaboyedoff et al., 2012) because they assign a single Z elevation to a point (defined by X, Y coordinates), excluding the possibility that the point has multiple Z values. Furthermore, rasterized DEMs will require very high grid densities to capture topographic change within the detail available in the original point data, but DEMs created at high resolution will have areas highly dependent upon point interpolation processes, where the point cloud densities are lower. TINs have similar problems where large triangles are created in zones of low point density.

* Corresponding author.
E-mail addresses: natan.micheletti@unil.ch (N. Micheletti), marj.tonini@unil.ch (M. Tonini), stuart.lane@unil.ch (S. Lane).

http://dx.doi.org/10.1016/j.geomorph.2016.11.016
0169-555X/

For these reasons, it is appropriate to develop change detection methods based upon the direct analysis of the point clouds using semi-automatic or automatic methods to detect and extract individual features. The latter have been proposed recently, notably for rockfall detection and rock mass structure analysis (Brodu and Lague, 2012; Gigli and Casagli, 2011; Riquelme et al., 2014; Rohmer and Dewez, 2015; Tonini and Abellan, 2014). In particular, in a previous work Tonini and Abellan (2014) developed a procedure similar to the one illustrated in the present study to detect rockfall from terrestrial LiDAR surveys. The vertical geometry of the analysed cliff allowed authors to reduce the spatial dimensionality of the geological point process and to adopt a 2D approach focusing their analyses on areal feature. Concretely, there are only few examples of the application of cluster-based methods to detect mass movements in geomorphology including volume calculation (e.g. Olsen et al., 2015).

The aim of this paper is to develop and apply a semi-automated method for isolating and identifying features of topographic change (erosion and deposition, or apparent changes caused by surface displacements) directly from point cloud data using a 3D clustering algorithm. This research does not aim at testing every possible algorithm available, but rather to evaluate the potential of clustering approaches for topographical data processing in geomorphology. Specifically, we tested the Density-Based Spatial Clustering of Applications with Noise (DBSCAN; Ester et al., 1996) for isolating mass movements from TLS-generated point clouds. The novelty of the proposed approach consists in the implementation of the DBSCAN 3D-module for the direct detection of mass movements from point clouds, without the need for interpolation as for a typical DEM to DEM comparison procedure. The resulting 3D-punctual features allowed the detection of topographic change with high precision, providing more accurate masking for the estimation of the volumes of the single erosion, deposition and front advancement units. The only factor that influences the detection of morphological change is the density of the original TLS data. We developed the method for a classic example of a geomorphic system that has been studied using TLS (e.g. Avian et al., 2009; Bauer et al., 2003; Bodin and Schoeneich, 2008): rock glaciers.

2. Case study: the Tsarmine rock glacier

The proposed methodology was developed for a very active rock glacier front (surface displacements in the order of meters per year; Barboux et al., 2014; Micheletti et al., 2015) located in the Swiss Alps: the Tsarmine rock glacier. Generally speaking, active rock glaciers act as sediment conveyors able to transfer large quantities of rock debris downward by permafrost-related creep (Delaloye et al., 2010; Gärtner-Roer, 2012). Their velocities may vary from a few centimeters to several meters per year (Barboux et al., 2014; Lambiel et al., 2008). Alpine rock glaciers are widely recognized as a primary agent in gravitational processes, including rockfalls and debris flows, as a result of their steep and unstable fronts (Harris et al., 2009; Kääb et al., 2007; Lugon and Stoffel, 2010). As a consequence, monitoring and quantifying their dynamics is of great interest, particularly in the face of climate change that could potentially enhance downslope displacement rates or reduce stability of the front slope (e.g. Kääb et al., 2007; Lugon and Stoffel, 2010; Micheletti et al., 2015).

The Tsarmine rock glacier is located in the Hérens Valley, in the Western Swiss Alps (Fig. 1). Its front is located at 2480 m a.s.l. (near the regional lower limit of permafrost; Lambiel and Reynard, 2001) and it is steep, devoid of vegetation and unstable. From the front, there is the regular detachment of debris, with delivery to a steep corridor containing a small stream. Deposits of boulders are visible for several hundred meters downstream.

The kinematics of the Tsarmine rock glacier have been investigated using archival aerial photogrammetry, differential SAR interferometry (DInSAR), differential GPS and fixed GPS measurements (Barboux et al., 2014; Delaloye et al., 2010; Lambiel et al., 2008; Micheletti et al., 2015). Rapid displacements, of the order of 1 to 2 m yr^{-1}, were measured during the years 1990s and 2000s

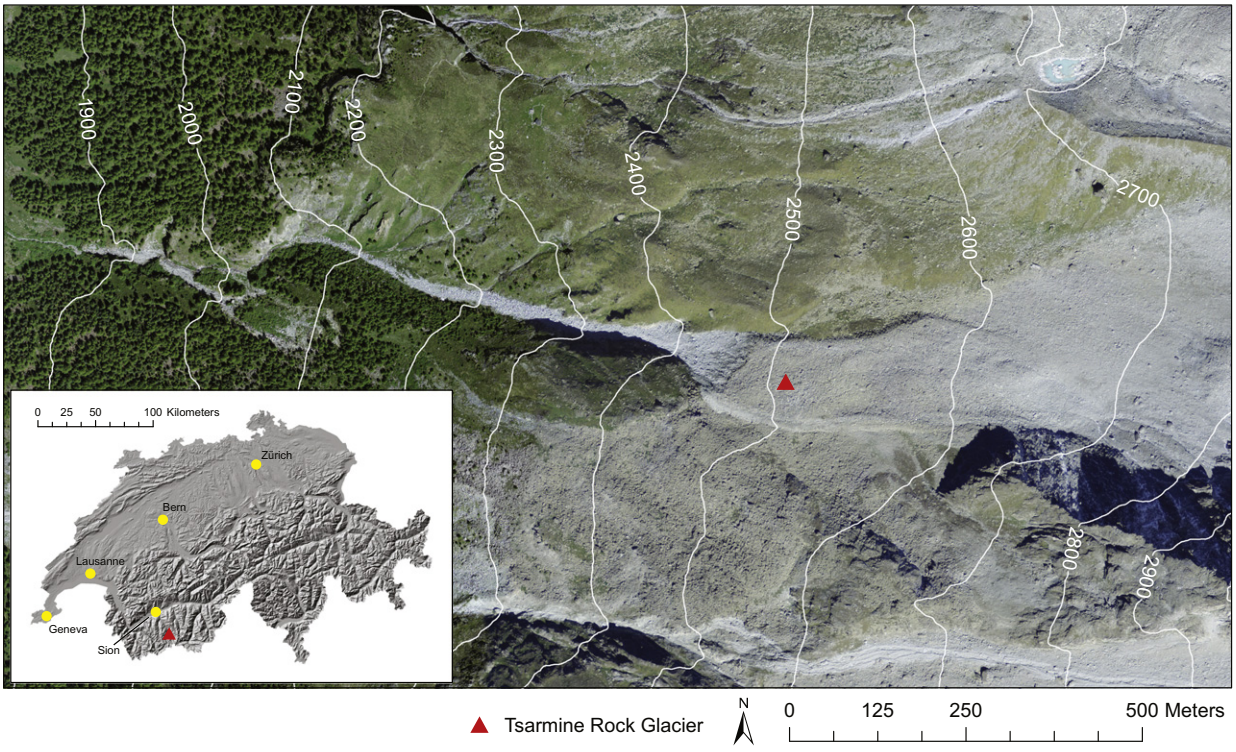

Fig. 1. The Tsarmine rock glacier, located in the Hérens Valley, in the Western Swiss Alps.
Source: Aerial photograph and relief shaded: Swisstopo

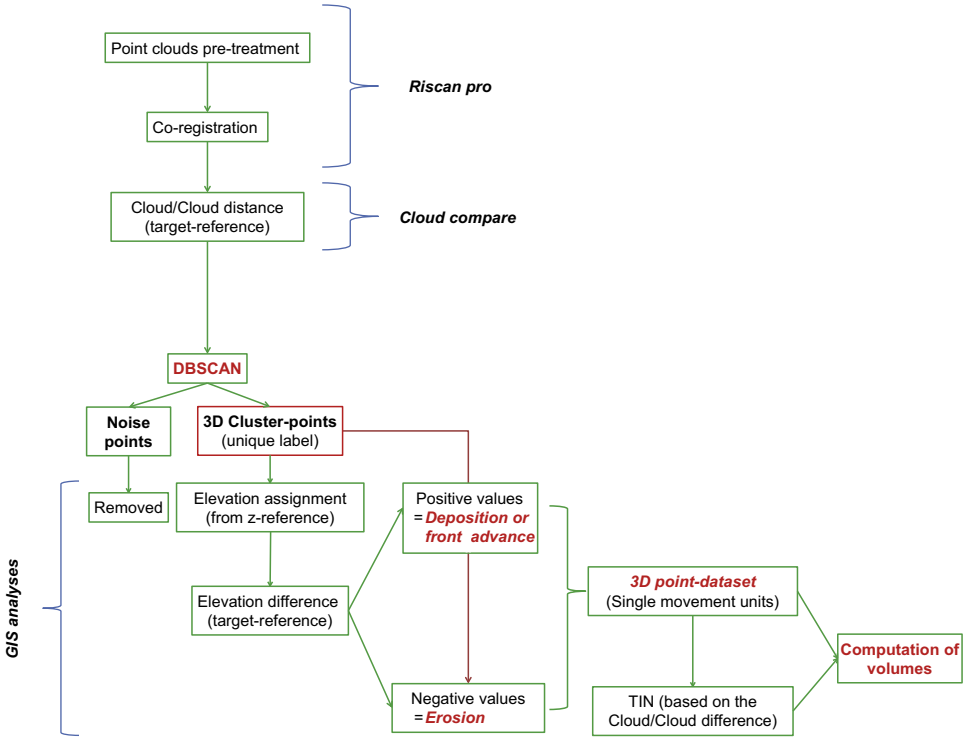

Fig. 2. The workflow of the stepwise analysis for a single time-step. For each time-step analysed, the target and reference point clouds are defined as explained in Section 3.3.

(Barboux et al., 2014; Micheletti et al., 2015). Following the rock glacier classification proposed by Lambiel et al. (2008), the Tsarmine rock glacier might be considered very rapid and susceptible to very frequent destabilization. Recent GPS data suggest an apparent acceleration since the summer of 2012. The body of the rock glacier has advanced at velocities of c. 4 m yr^{-1} in recent years, with peaks up to 6 m yr^{-1} in 2015 (unpublished data, Universities of Lausanne and Fribourg). Because of this exceptionally high displacement rate, the Tsarmine rock glacier is likely to be associated with considerable geomorphic change at its front, even over short time-scales. As a consequence, it represents an ideal candidate for developing our method.

3. Methodology

Fig. 2 gives an overview of the methodology, from data acquisition through to computation of the volume of change associated with each detected movement units (i.e. erosion and deposition/advancement movements). In summary: (1) point clouds were generated using a TLS on a number of dates (see Section 3.2); (2) these clouds were co-registered using stable zones within the surveyed area (bedrock outcrops, verified as stable at decadal scale, see Micheletti et al., 2015); (3) Using a threshold value, points where there may have been some topographical change were identified; (4) these retained points were subjected to a density based clustering algorithm, DBSCAN, which aimed at grouping cluster-points into single features and filtering out noise points, found in low-density regions; (5) the detected features were then labeled as clusters of material loss or gain according to the elevation assignment of the change; and (6) the volume of change was finally calculated for each cluster by a triangulation process.

3.1. DBSCAN: 3-D density based clustering method

The clustering algorithm DBSCAN (Density-Based Spatial Clustering of Applications with Noise; Campello et al., 2013; Ester et al., 1996) was used to classify points within the clouds into single cluster features. The computational environment to perform the analysis was the open source R programming language (R Core Team, 2015), using the dbscan package (Hahsler et al., 2016). This procedure allows identification of clusters of arbitrary shape in 2D or 3D space on the base of the local density of points. Essentially, points that are close together are grouped into the same cluster, while points isolated or in very low-density regions are labelled as noise. Only two parameters are required to perform this classification (Fig. 3): the neighbourhood size epsilon (*eps*) and the minimum number of points necessary to form a cluster (*MinPts*). On the basis of these two parameters, the algorithm explores each point in the cloud, counting the number of the neighbouring points falling within a circle (for the 2D model) or a sphere (for the 3D model) of radius equal to the *eps*-value: if this number is equal to or greater than *MinPts*, the group of points is labelled as a cluster. The same identifier is attributed to points belonging to the same cluster so that each single cluster is univocally recognized. Points which do not satisfy the *MinPts* criteria are classified as noise (see Fig. 3). The central point of each identified cluster is called *core*-point. Then, as some points in the pattern can be density-reachable by more than one *core*-point, they belong to more than one cluster. These are called *seed*-points. The corresponding *core*-points of clusters connected by *seed*-points are said to be density-connected to each other and their clusters blended together to form a unique cluster feature of arbitrary shape.

The two parameters *eps* and *MinPts* greatly affect the shape, size and number of clusters detected by the algorithm. Their choice mainly relies on a decision that has to be taken as to whether the objective is to identify a large number of small clusters or a small number of large clusters within the original dataset. The default value for *MinPts* in the used package is 5 (Campello et al., 2013). The actual value used should reflect: (1) the characteristics of the dataset, as when working with very large datasets with high density of points, higher values may need to be set to remove noise; and (2) the surface being considered which will determine the spatial scale of single movement units, and hence the point density that should

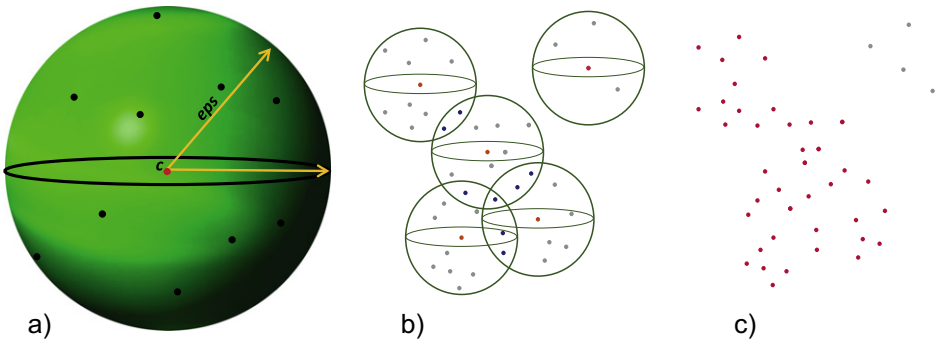

Fig. 3. (a) Computation of the number of points at a maximum distance (*eps*) around a core-point (*c*): if *MinPts* condition is satisfied they form a cluster (here *MinPts*=10); (b) core-points are density-connected by the chain of intermediate seed-points (blue dots); and (c) their clusters blend together to form a unique cluster feature of arbitrary shape (red point cloud) while grey points represent noise.

be needed to define geomorphological features. Once that the *MinPts* parameter has been fixed, a suitable value for the *eps* neighbourhood size can be deducted using a k-nearest neighbours (k-NN) distance graph, that is plotting the distance to the k-nearest neighbour and imposing *k* as equal to *MinPts*. The optimal *eps*-value should coincide with the strong curvature in the plot: smaller values should give rise to an excessive fragmentation with small clusters dispersed among isolated noise-points; for larger values, the majority of the detected clusters will blend together to form huge cluster features.

3.2. Field campaign

An ultra-long range LiDAR RIEGL VZ-6000 scanner was employed to acquire sequential 3D datasets of the rock glacier front. This high speed, high precision device has proven very efficient for geomorphological research (e.g. Fischer et al., 2016; Gabbud et al., 2015). By means of its long-range capability (up to 6000 m), the use of this device allowed the scan position to be set on the opposite side of the valley facing the rock glacier (c. 2800 m of flying distance, see Fig. 4), yielding to minimal occlusion effect. TLS scans were performed on four different dates over two consecutive summers: a first survey was carried out on the 23th of September 2014, while three more were completed on the 29th of June, the 20th of July and the 22th of September 2015. As it is routine in TLS surveys, the laser device was placed on a tripod over stable ground. The same approximate instrument position was used for each survey. The laser pulse repetition frequency was reduced to its minimal value (30 kHz) to prevent range ambiguity. Vertical and horizontal angle increments were both set to 0.004°, except for the 2014 survey where a value of 0.0045° was chosen (resulting in slightly lower expected point densities). For registration purposes, a very large area containing extensive stable zones (i.e. bedrock outcrops, verified as stable at decadal scale, see Micheletti et al., 2015) in addition to the rock glacier was scanned. The RIEGL VZ-6000 is equipped with on-board inclination sensors, meaning that even when not geo-referenced, the inclination data can be used to obtain datasets where the *Z* dimension represents the elevation above the *X*-*Y* plane. An example of the point cloud appearance at the rock glacier front is shown in the detail of Fig. 4.

3.3. Point cloud pre-treatment and co-registration

TLS data were imported and processed initially using the software RiSCAN PRO. The first step was the manual removal of non-ground surface points, caused by atmospheric reflections due to dust or moisture. Afterwards, a relative registration of point clouds was necessary to co-register the four surveys into a common coordinate system. The most recent data (the 22th of September 2015) were treated as the reference surface. Surfaces prone to considerable topographic change (including the rock glacier) were identified and excluded from the co-registration procedure. A coarse, approximate registration was achieved by manually identifying corresponding points between the reference surface and each point cloud and shifting the latter by modifying a matrix defining the sensor orientation and position proper to each survey dataset. Subsequently, the co-registration was refined using the Multi-Station Adjustment (MSA) RiSCAN PRO function. The latter uses an Iterative Closest Point (ICP) method (e.g. Zhang, 1994). In the ICP, the orientation and the position of scan positions is modified using least-squares minimization of residuals in order to calculate the best overall fit in respect to the

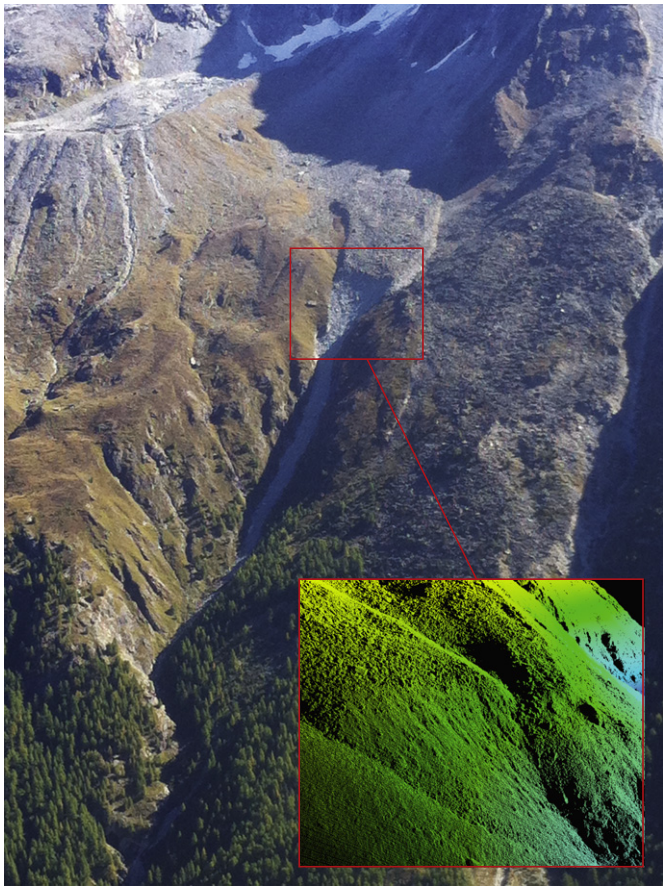

Fig. 4. The Tsarmine rock glacier and the steep corridor below its front, as visible from the scanning site on the opposite valley side. The detail shows the point cloud of the rock glacier front (survey: 22/09/2015); the front width is c. 100m.

reference surface. Each residual is defined as the distance between each data point in the cloud being co-registered and its closest point in the reference surface. At every iteration of this process, the user is required to update the nearest point search (e.g. the search radius) and the adjustment parameters (minimum change of error to stop the calculations). After a number of iteration the best fit is determined, and the residual distances are calculated and used to assess the quality of co-registration. For all co-registered scans, the residual distances have a Gaussian distribution with mean of zero. Thus, the precision of the co-registration procedure could be evaluated by the standard deviation of the residual distances (σMSA - Multi-Station Adjustment): in our case it ranged from $\pm$0.0598 to $\pm$0.0987 m.

After co-registration, a mask was used to restrict point clouds to the area of interest: the front of the rock glacier and the corridor below. The point density in the area of interest was c. 24 p m^{-2} for 2015 surveys and 12 p m^{-2} for the 2014 one. The clustering algorithm (DBSCAN) requires as input a 3D dataset, which in our case consists of the point cloud and displacement distance, the latter measured as a Euclidean distance. For any two co-registered datasets, we set the sequentially first dataset as the target and the more recent dataset as the reference. For each point in the target cloud it is necessary to identify its corresponding nearest point in the reference cloud, referred to as the Cloud/Cloud difference (Table 1). Consequently, datasets were compared using the distance tool in the point cloud data management software Cloud Compare (EDF R&D, 2012), freely available at http://www.danielgm.net/cc. This tool exploits a chamfer matching algorithm (Barrow et al., 1977) to obtain the three-dimensional (Euclidean) distance between each point in the target dataset with its closest point in the reference dataset.

These distances comprise two components: (1) real material loss/gain signals; and (2) noise associated with the fact that points of two datasets of different epochs are not exactly co-located, because of sampling or co-registration errors. In practice, as the MSA used zones of no change, the residual distances for these zones are a measure of the noise in the data (i.e. σMSA). The question then becomes what multiple of σMSA to use. One option is to apply some kind of statistical confidence to the distances determined (e.g. in 3D application $\pm$1.614σMSA gives a 95% confidence that the distance is a signal and not noise; Lane et al., 2003). However, if densities are spatially variable within the zone of interest, or between the zones used for the MSA and the zone of interest, such precision may be misleading. One alternative is to take a process-based definition. Here, we note from field observations that the size of displaced boulders is typically $>$ 0.30 m and we use this as a change criteria: that is a boulder must move through its own volume to be considered a change. For comparison, 0.30 m is approximately 3σMSA, approximately a 99.5% confidence level.

3.4. Choice of DBSCAN parameters

In the present study, the minimum number of points to constitute a cluster was fixed first, and then the plot of the k-nearest neighbour (k-NN) distance was used to find a suitable value for the *eps* neighbourhood size. To test the influence of DBSCAN parameters on cluster identification, the one month scan (Table 1) was used. First, we applied increasing values of *MinPts* (the default of 5, and 10, 15 and 20) to determine the value more appropriate to our case study. We defined k-NN plots for each *MinPts* value, using the plot curvature to identify the optimal *eps*-distance to the *k*th nearest neighbour. Second, to evaluate if the value corresponding to the strong curvature of the k-NN plot is effectively the best choice, we kept *MinPts* equal to the value judged more appropriate (in our case 10) in terms of number of clusters and percentage of noise, and we explored the effects caused by different *eps*-values.

Table 1
LiDAR scans and their use as target and reference datasets in the analyses.

Target	Reference	Time-step
29/06/2015	20/07/2015	1 month
20/07/2015	22/09/2015	2 months
29/06/2015	22/09/2015	3 months
23/09/2014	22/09/2015	1 year

3.5. Determination of volumes of loss or gain of material

The DBSCAN algorithm provided a dataset containing the following components: the x, y, and z-coordinates of each point plus an integer vector assigning it to either a particular cluster feature or, for the value 0, as an isolated noise point. Then a stepwise GIS analysis was performed to discriminate between single movement units of erosion and deposition, and for the determination of their volumes. This was achieved by using the rasterized DEMs of the reference datasets (computed here at 0.5 m resolution) and assigning the sign of the elevation difference, designating material loss or gain, to each single cluster-point. This rasterization is unfortunately necessary to discriminate positive and negative changes, but should not affect significantly the results as change identification and further calculation are based solely on DBSCAN outputs. In fact, by this procedure single cluster features resulting from DBSCAN could be split into different movement units. Finally, the computation of the volumes of each single erosion and deposition/front advancement unit was achieved by creating a TIN surface in the XY plane based on the value of the Cloud/Cloud difference (the distance of the closest point in the reference dataset).

3.6. Confront with traditional DEM-to-DEM approaches

In a final stage, the volumes obtained with the proposed procedure, were compared with ones obtained by the traditional, rasterized, DEM comparison approach, focusing on the one month time lapse. The target (June 2015) and reference (July 2015) co-registered point clouds were interpolated to a 0.3 m regular grid. Given the high point density, a nearest neighbour interpolation was deemed sufficient for that purpose. The subtraction between two raster DEMs is traditionally used to detect elevation changes. To isolate real change from noise induced by the data or the interpolation procedure, we could follow the error propagation proposed by Lane et al. (2003). A 95% confidence limit would provide a detection limit of $\pm$0.27 m, very close to the 0.3 m value used for noise removal. Hence the detection limit used was rounded up to use the same value.

4. Results

4.1. Choice of DBSCAN parameters

The k-distance graphs obtained by applying *MinPts* equal to 5, 10, 15 and 20 (see example in Fig. 5) indicated that the related optimal *eps*-values, coinciding with the strong curvature of the plot, also increase from 0.8 up to 1.5 m, approximately linearly. By fixing *MinPts* as equal to 10, values of 0.5, 1.5 and 2 m for *eps* were tested against the allegedly best one of 1 m (Fig. 5). Table 2 shows the results obtained by applying these DBSCAN parameters on the number of clusters identified, the percentage of points labelled as noise, and the volume of change that results.

Volumetric estimations do not seem to be particularly sensitive to the tested DBSCAN parameters. This is notably the case for the *MinPts* parameter and while the number of identified clusters changes substantially, the percentage of points classified as noise changes much less. Thus, the effect of *MinPts* is primarily upon the number of cluster but not upon the total number of points that belong to a clusters. In our case 10 gives the best results: the default 5 value generate many small clusters, while applying higher vales (15 and 20) it results a

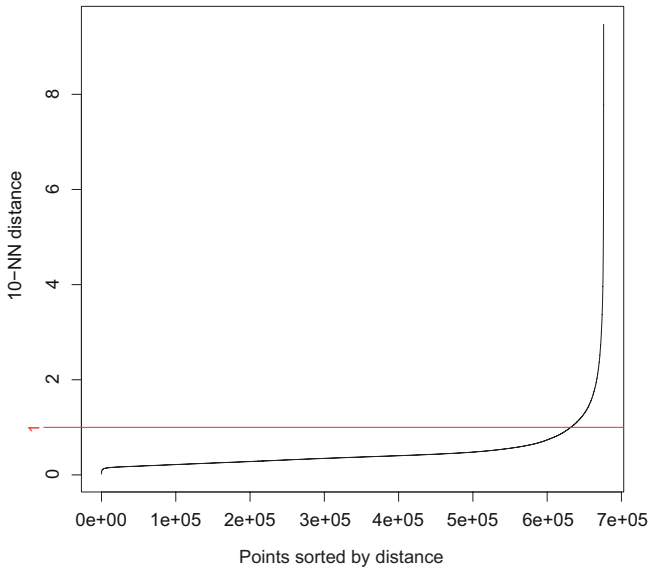

Fig. 5. Example of optimal *eps* value retrieved using k-NN plots for *MinPts* equal to 10.

huge aggregation of the previously detected single clusters. When the *MinPts* is set to 10 and the *eps* parameter is varied, the number of clusters changes more dramatically, and so does the percentage of points identified as noise. It is then not surprising that the volumes of change are more sensitive to different values of *eps* than when the *MinPts* parameter is varied (Table 2).

To resume, from our analyses it results that the best value for *MinPts* is 10 and that different values have to be tested case by case to avoid aggregation or fragmentation effects. We also proved that the strong curvature of the k-NN plot is a good tool to determine the optimal *eps*-distance. These parameters describe very well the underling geomorphological process: in fact mass movements appear to be micro-topography controlled, with a length scale of about 1 m, which confirm 1 m value as optimal for *eps*.

4.2. Effect on volumetric calculations

The GIS analyses allowed the computation of the volumes of the erosion and deposition/advancement movements. Results are shown on Table 3 and summarize the geomorphological activity at the Tsarmine rock glacier during the summer 2015 (one, two and three month time-steps) and during one entire year (September 2014 to September 2015). The number detected movements oscillates between 410 and 543, while the total volume of geomorphological change (V_{TOT}) consistently increases as time intervals increase. This implies that over the longer term bigger clusters of geomorphological activity are being identified, which is the expected outcome, also reflected in no real evolution in the number of clusters. Generally, estimates of eroded (V_E) and accumulated (V_D) volumes are balanced at short time scales (one and two months), as one would expect. However, material gain volumes dominate at the longer time span. A possible explanation lies in the fact that the front invariably advances under the influence of creep-related deformation in the rock glacier body. The process is slow and continual, and permafrost thaw and rock fall at the front mitigates it, but at longer timescales it is possible that a part of the front has not yet collapsed, and the advance become visible as an apparent gain of material. Another consequence is the reduction or suppression of the volumes of collapsed material that can be observed, as the void might be masked by front advance. Consequently, results should tend to slightly overestimate the total accumulation and underestimate eroded volumes. These processes are likely to be relevant at intermediate and long timescales (e.g. three months and one year, Fig. 8b and c), and explain (i) the unbalance between V_E and V_D at these timescales, and (ii) the disagreement between the sum of eroded volumes (V_E) for one and two months and three month erosion.

Fig. 7 compares the maps of erosion and deposition/front advancement units obtained by applying DBSCAN with the results generated using a traditional, rasterized, DEM comparison (0.3 m resolution). At one level, the patterns are very similar. The same areas are highlighted as material loss and gain, although the rasterized DEM of difference has more scattered, isolated changes as the comparison makes no reference to the extent to which the data are coherently organized. However, volumetric estimations with DEM comparison are three times higher than with the 3D-clustering approach (see Table 3), with values for one month close to what would be expected to be observed in one year. These volumetric changes appear unrealistic at the timescale of one month for the presented case study. We attribute this to the effect of artificial surface differences associated with point density effects. Point interpolation assigns an elevation to every grid point and then every grid point is compared, giving a change if it is greater than the 0.3 m detection limit used here. No reference is made to the coherence of changes by association to adjacent points. Given the complex surface variability, interpolation to grids may cause isolated elevation changes that are a result of the chance inclusion of topographic highs and lows in the interpolation surface, rather than any actual geomorphic change. These changes are filtered out by DBSCAN since the original points are labelled as noise. More generally, whether or not a clustering algorithm is used, meaningful detection of surface change should consider the spatial coherence of the change, with respect to the known spatial variability within the surface. Despite a ground

Table 2
Sensitivity of the resulting number of cluster features and total volumes V_{TOT}, volumes of erosion V_E and deposition/front advancement V_D to changes in the DBSCAN parameters. The effect of parameter settings on aggregation and disaggregation of clusters is shown in Fig. 6. In bold: retained DBSCAN parameter set.

Set of DBSCAN parameter	*MinPts*[a]	*Eps* [m]	No. of cluster features	Noise points [%]	V_{TOT} [m^3]	V_E [m^3]	V_D [m^3]	V_{TOT} change [%]
a) Increasing MinPts, Optimal eps								
1	5	0.8	695	5.0	761	320	441	+3.1
2	**10**	**1**	**327**	**6.8**	**738**	**313**	**425**	**Ref.**
3	15	1.3	159	6.3	748	316	432	+1.3
4	20	1.5	108	6.5	747	315	432	+1.2
b) Constant MinPts, Increasing eps								
1	10	0.5	751	22.7	658	290	368	−11.0
2	**10**	**1**	**327**	**6.8**	**738**	**313**	**425**	**Ref.**
3	10	1.5	149	2.7	788	330	458	+6.8
4	10	2	86	1.3	808	338	470	+9.5

[a] DBSCAN default MinPts value: 10.

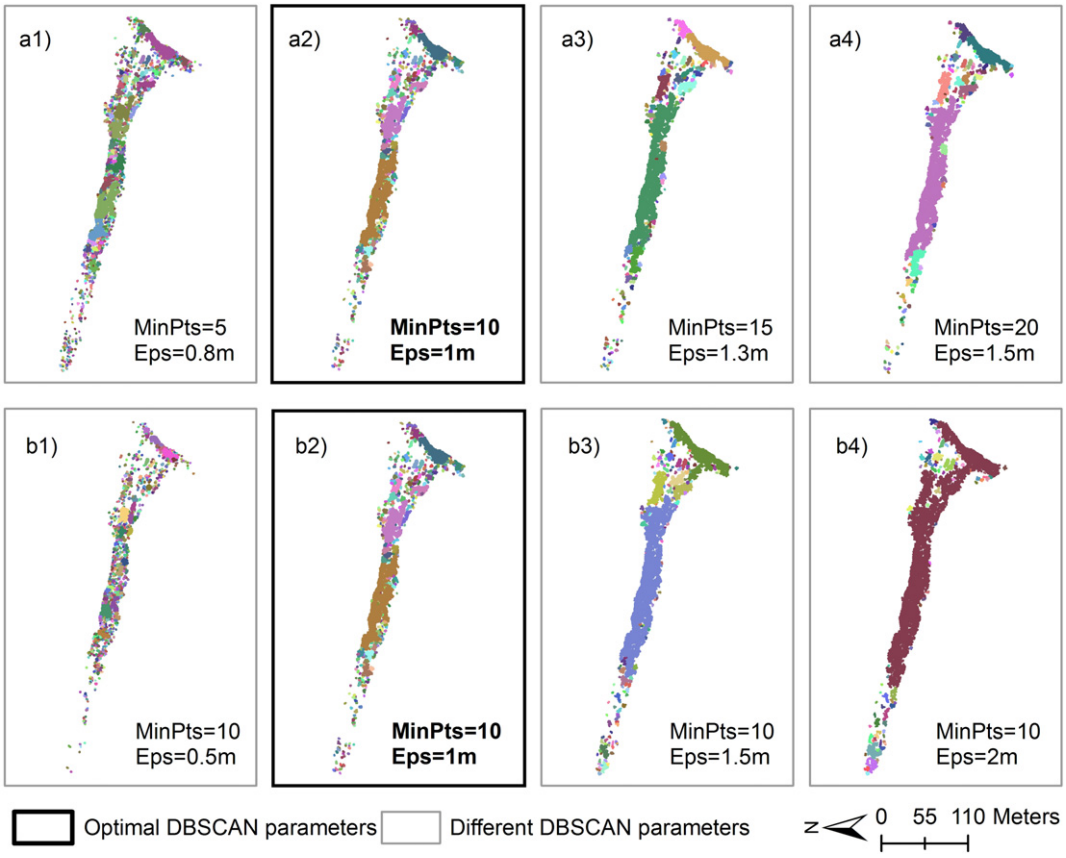

Fig. 6. Sensitivity of the cluster aggregation/disaggregation to changes in the DBSCAN parameters (see Table 2).

truth to determine the actual volumetric change cannot be acquired for this type of application, the striking differences between the two approaches indicate that carefulness is always necessary when an estimation of volumes is performed from topographic data, with any method.

5. Discussion

5.1. Merits of a 3D-clustering approach

TLS for data acquisition has developed rapidly in recent years. The outputs of this procedures (i.e. 3D point clouds) are widely used in the geosciences (Abellan et al., 2016) and developing new and fast algorithms for feature extraction is crucial in this context. Our approach, based on a density clustering method, proved to be very useful for detecting movement units (i.e. features of material loss and gain) at a rock glacier front. The same procedure can be applied to extract 3D features related to any landform or geomorphologic process such as rockfall, debris flows, and landslide. As with similar methodologies based upon using point clouds for feature detection (Olsen et al., 2015; Riquelme et al., 2014; Tonini and Abellan, 2014), our approach leads to a reduction in noise and to clustering of points into individual features. Nonetheless, in comparison with existing applications it has some advantages. First, the processing speed is very fast, notably the most recent version of the dbscan package (Hahsler et al., 2016). Second, by adopting the 3D module, clustering algorithms can be applied to any surface regardless of local topographic slope. For example, on steep mountain sides, lateral point displacement might be reduced, with vertical point displacement becoming important, thus emphasizing the need for a 3D rather than a 2D approach. Third, the proposed methods permitted the isolation of cluster features directly from point clouds, allowing precise change masking and reaching a precision in the following computation of the volumes that depends mainly on the actual registered distance between points and is not affected by prior interpolation.

Table 3
Synthesis of the geomorphological activity (deposition or material gain from front advance (D) and erosion (E) movements) at the Tsarmine rock glacier during the summer 2015 and between Sept. 2014 and Sept. 2015. Volumes (V) in m^3.

Time-step	Number of clusters	V_{TOT} [m^3]	V_E [m^3]	V_D [m^3]
1 month	484	738	313	425
2 months	543	826	410	416
3 months	410	1376	536	840
1 year	538	2056	724	1332
1 month[a]	–	2079	1014	1065

[a] Traditional DEM comparison.

5.2. Geomorphological activity at the rock glacier front

Fig. 8 illustrates the clusters identified by DBSCAN, where each color corresponds to a unit of morphological change. The geomorphological activity during a time-step of one month in the summer 2015 highlights a major cluster with diverse smaller ones at the rock glacier front (Fig. 8a, 1). From 100 m downslope, an area of deposition is characterized by the presence of two particularly large clusters (Fig. 8a, 2). In the lower part of the area of study, very small clusters are observed (Fig. 8a, 3). These are likely to be single boulders that were able to move farther downslope in the channel.

Clusters identified over a time-step of three months (Fig. 8b) appear larger at the rock glacier front, although they do not seem to be more numerous. Despite their proximity, the two major clusters are not unified (Fig. 8b, 4). The central part of the slope seems

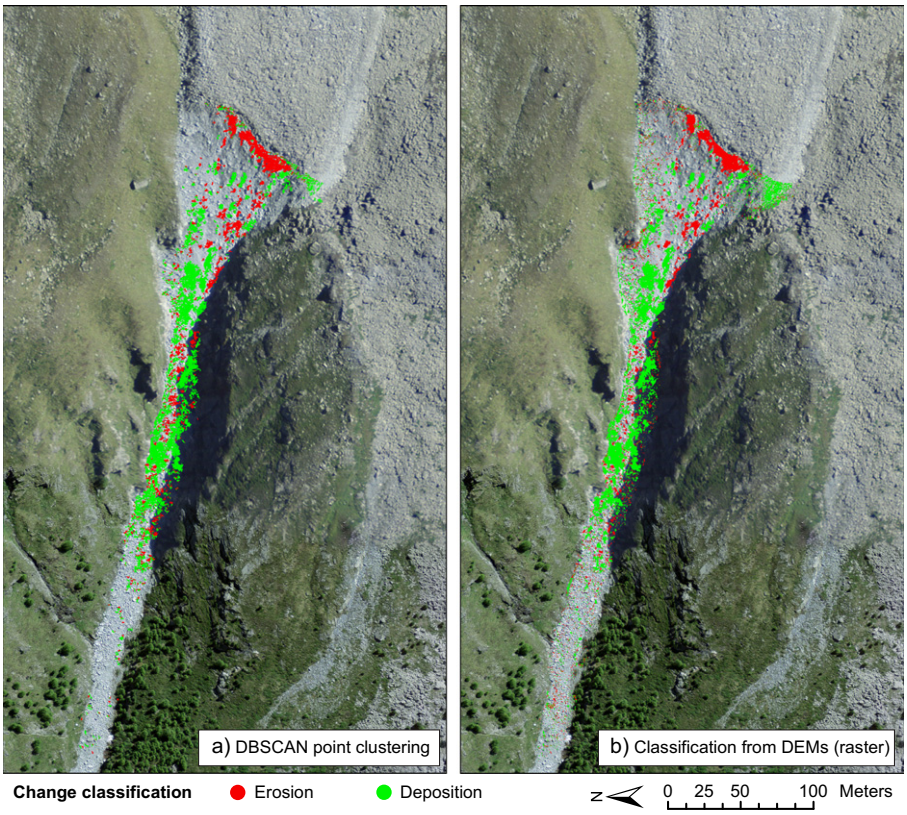

Fig. 7. Comparison for one month data between a) DBSCAN point clusters (VTOT = 738 m^3) and b) erosion and deposition patters classified from rasterized DEM comparison (VTOT = 2037 m^3).

slightly more fragmented, although two very large clusters are once again visible (Fig. 8b, 5). Larger clusters are featured in the lower part of the study area in comparison with the shorter timescale analysis, indicating that several boulders reached that zone (Fig. 8b, 6).

One-year clusters are shown in Fig. 8c. Almost the whole front surface has undergone change, as indicated by various large clusters (Fig. 8c, 7). The middle part of the area of interest has almost completely changed as well, as testified by the presence of many clusters

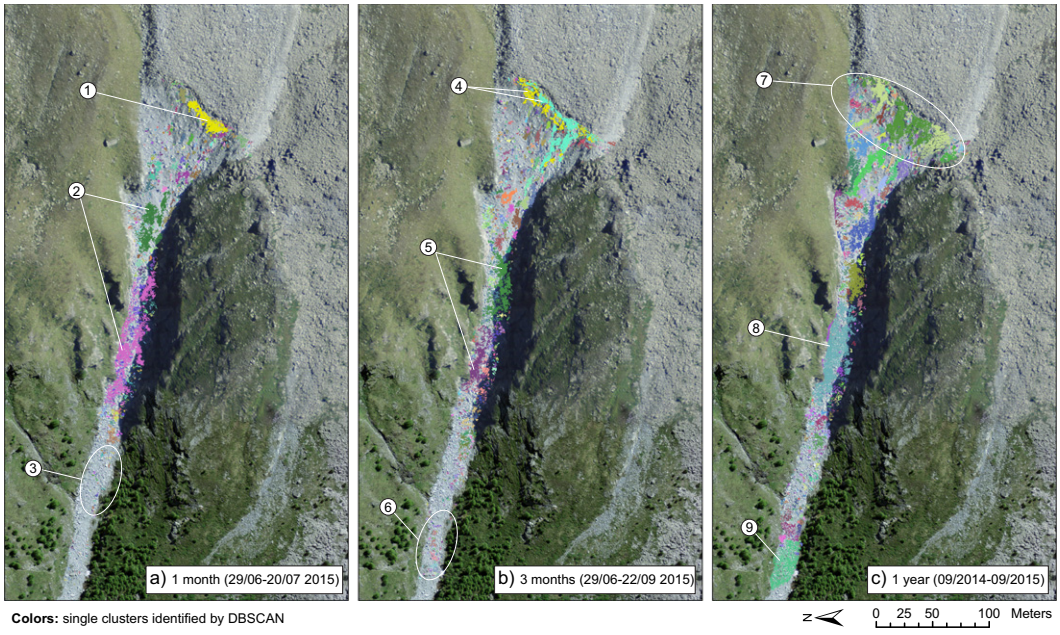

Fig. 8. Three-dimensional geomorphological changes identified using DBSCAN for a) one and b) three months and c) one year time lapses. The color of the dots represents single features of material gain or loss. Numbers are referred to in the text.

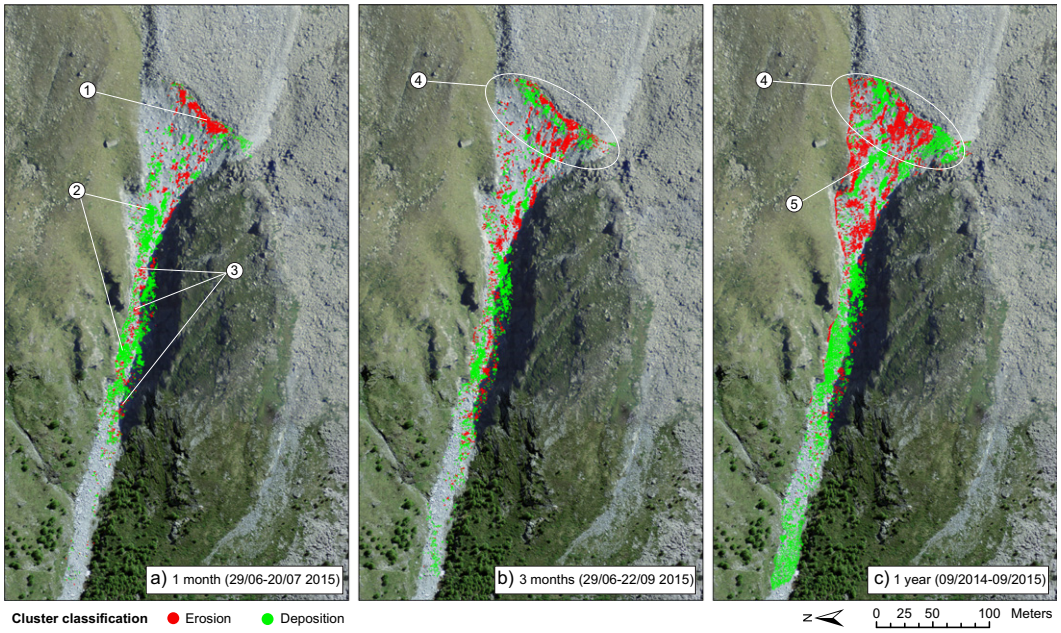

Fig. 9. Deposition, front movement and erosion features for the field campaigns corresponding to a) one and b) three months and c) one year time lapses. Numbers are referred to in the text.

including a very large one (Fig. 8c, 8). In the lower part, small clusters precede another very large one, depicted in green (Fig. 8c, 9).

The clusters presented in Fig. 8 are then classified as material gain or loss following the procedure discussed in Section 3.5 (Fig. 9). This demonstrates that the largest cluster visible at the front at the one-month time-step is because of a collapse event which occurred in July 2015 (Fig. 9a, 1). The remaining features in this zone are a mixture of erosion and deposition, probably caused by detached material blocked by other boulders and unable to travel farther. As expected, the vast majority of clusters in the channel are depositional (Fig. 9a, 2). Erosional footprints in that zone are scattered but exist (e.g. Fig. 9a, 3), indicating potential remobilization of material or incision.

Fig. 9b shows that the two major and separated front clusters at the three month time-scale are opposite in nature (Fig. 9b, 4). The fact that the erosional cluster is located above the deposition area allows two hypotheses. On the one hand, the eroded material could have simply slid from the upper part of the detachment niche without leaving the rock glacier front. On the other hand, the two clusters could be unrelated; in that case the eroded material has likely left the front area, and the material-gain pattern could be because of the front advance caused by deformation-related creep in the rock glacier body. Given the scale of the analysis (three months) and the seasonal conditions (summer, affected by a heat wave), this second scenario appears more realistic. The front is also characterized by the presence of many erosional clusters with elongated shapes, very likely caused by collapse and consequent transit of material downstream. Spatial patterns in the channel are similar to the one-month application, but material is deposited further downstream in this case.

The geomorphological activity at the rock glacier front over one year is almost equally divided into gain and loss of material (Fig. 9c, 4). While erosional patterns are proof of material collapsing as permafrost thaws, the green features in Fig. 9c, 4 are probably because of the rock glacier advancing. In that sense, deposition in these clusters is only apparent, as it is merely a displacement forward. Starting from only 50 m below the crowning of the front, depositional patterns could also be caused by material trapped after a collapse by cause of surface roughness; the elongated cluster in the centre could be an example (Fig. 9c, 5). Throughout the course of the channel, large clusters of deposition are visible.

MeteoSwiss (2016), in their annual climatic report, indicated that year 2015 was once again a record-year for measured air temperature. In particular, the summer 2015 was characterized by an extreme heat wave, and it is classified as the second warmest summer in Switzerland since the beginning of measurements, 152 years ago. Beaten only by the extreme summer of 2003, it registered between 2 and 2.5 °C more than the norm 1981–2010 (MeteoSwiss, 2016). As a permafrost-related process, rock glacier creep is supposedly very sensitive, among others controlling factors, to temperature forcing (e.g. Kellerer-Pirklbauer and Kaufmann, 2012).

The results achieved in this study offer detailed information on the dynamics of the Tsarmine rock glacier front during the hot summer of 2015. During only about one month, 313 m^3 of erosion occurred in the investigated zone. The two month results display slightly higher values: 410 m^3. For both periods, little more than 400 m^3 of accumulated material are estimated. The superior geomorphological activity in the shorter, earlier time span could be an indication of the crucial role of snowmelt, which generally occurs around June for this elevation and orientation, in eroding and mobilizing boulders at the rock glacier front. Another reason could be a strong capacity of thawing at the front that manifests at the beginning of the summer season.

Analysis of the June and September 2015 LiDAR datasets resulted in an estimated 536 m^3 of erosion. It could be argued with confidence that this result is an underestimation. GPS measurements indicate that the rock glacier surface moved at a velocity of almost 5 m yr^{-1} during that period, which correspond to a net advance of 1.25 m. This process partially conceals collapse events by causing the front to advance and occupy the space left empty. The volume of eroded material should be at least a few hundred cubic meters more. The same is true for volumetric estimations for one year (September to September). We argue that erosion quantities (724 m^3) are strongly underestimated for the same reason, as confirmed by accumulation volumes that are almost double of them (1332 m^3, excluding material that traveled further downstream). While an accurate estimation

could not be formulated, it is realistic to assume that the rock glacier front delivers sediments downstream in the order of c. 1500 m^3 yr^{-1}.

The mass transfer occurred at the Tsarmine rock glacier front during the hot summer 2015 appears extremely high, a fact that could be attributed to the exceptionally high mean velocities observed in the last couple of years (c. 4 m yr^{-1}). These are considerably higher than the kinematics estimated for the beginning of the 2000s (1 to 2 m yr^{-1}; Barboux et al., 2014; Micheletti et al., 2015), which nonetheless included the 2003 heat wave, suggesting that sediment delivery rates might be much higher today in comparison with 10–15 years ago. In this regard, Gärtner-Roer (2012) observed, for a very active rock glacier located in an adjacent valley (the Turtmann Valley), maximum velocities of 2.59 m yr^{-1} during the heat wave of the summer 2003, with a corresponding peak of sediment transfer rate of 1.1 Mt yr^{-1} (corresponding to c. 415 m^3 yr^{-1} if a specific weight of 2.65 t m^{-3} is considered; Barsch, 1977). For a similar case study in the Mattertal Valley, Lugon and Stoffel (2010) encountered much slower kinematics at the beginning of the years 2000s, with maximum movement rates of 0.88 m yr^{-1}. They estimated a mass flux of 500–700 m^3 yr^{-1}, but corrected sediment delivery to 300–400 m^3 yr^{-1} because of the considerable amount of voids and ice contained in the rock glacier. Following these indication, it would be plausible to assume that erosion volumes at the Tsarmine rock glacier have almost double in the last decade. Comparing our results to the behavior of other rock glaciers during the hot summer of 2015 could provide insights in this sense.

The maps of erosion and deposition/front movement clusters (Figs. 8 and 9) illustrate the high geomorphological activity at the front of the rock glacier during the period of study. Nonetheless, boulders detaching from the front do not appear to travel far. Large clusters of deposition are identified a few hundred meters below the front, and with a few exceptions at longer time spans where traces of material extend farther downstream, boulders are exclusively stocked in the first 200 m of the channel. Hence, despite evidence of significant sediment production at the rock glacier front, impacts at the valley bottom are absent for the time being. A further remobilization of this material (e.g. by debris flows events) is not to be excluded, but the diameter of rocks is quite substantial and thus the risk quite mitigated.

6. Conclusions

The proposed method permitted detection of features of positive and negative change, their mapping and derivation of detailed volumetric change estimations for a rock glacier front located in the Swiss Alps. Single cluster features of erosion and deposition/front movements were extracted directly from point clouds, detected by DBSCAN without the necessity of interpolate the 3-D original data. This approach allows detecting realistic volumetric features, with change detection that depends only on the resolution of the TLS point cloud. Finally this methodology represents an alternative to traditional point cloud processing techniques for applications in geomorphology.

Remarkable geomorphological activity was observed at a rock glacier front during the summer of 2015, likely under the influence of the very rapid permafrost creep suggested by GPS measurements. To determine if the influence of the exceptionally high temperatures observed that season plays a driving role in these processes, TLS surveys for the following summers would be necessary, and the proposed approach would be ideal to efficiently process the resulting datasets. Moreover, a more detailed coupling between meteorological events, climatic data and morphological changes were beyond the focus of this study, but would need to be performed to infer the effects of external forcing on sediment production at a rock glacier front.

Acknowledgments

This research was supported by the Herbette Foundation of the University of Lausanne, the Canton Vaud, and the Canton Valais. We are very grateful to the University of Lausanne and the University of Fribourgfor funding the laser scanner device used in this study. We would like to thank Mario Kummert and Adnan Tahir for their valuable help in the field.

References

Abellan, A., Derron, M.H., Jaboyedoff, M., 2016. Use of 3D point clouds in geohazard" special issue: current challenges and future trends. Remote. Sens. 8 (130). http://dx.doi.org/10.3390/rs8020130.

Abellan, A., Oppikofer, T., Jaboyedoff, M., Rosser, N.J., Lim, M., Lato, M.J., 2014. Terrestrial laser scanning of rock slope instabilities. Earth Surf. Process. Landf. 39 (1), 80–97. http://dx.doi.org/10.1002/esp.3493.

Abellan, A., Vilaplana, J.M., Martinez, J., 2006. Application of a long-range terrestrial laser scanner to a detailed rockfall study at Vall de Núria (Eastern Pyrenees, Spain). Eng. Geol. 88 (3–4), 136–148. http://dx.doi.org/10.1016/j.enggeo.2006.09.012.

Alho, P., Kukko, A., Hyyppa, H., Kaartinen, H., Hyyppa, J., Jaakkola, A., 2009. Application fo boat-based laser scanning for river survey. Earth Surf. Process. Landf. 34 (13), 1831–1838. http://dx.doi.org/10.1002/esp.1879.

Anderson, E.S., Thompson, J.A., Crouse, D.A., Austin, R.E., 2006. Horizontal resolution and data density effects on remotely sensed LIDAR-based DEM. Geoderma 132 (3–4), 406–415. http://dx.doi.org/10.1016/j.geoderma.2005.06.004.

Avian, M., Kellerer-Pirklbauer, A., Bauer, A., 2009. LiDAR for monitoring mass movements in permafrost environments at the cirque Hinteres Langtal, Austria, between 2000 and 2008. Nat. Hazards Earth Syst. Sci. 9, 1087–1094. http://dx.doi.org/10.5194/nhess-9-1087-2009.

Barboux, C., Delaloye, R., Lambiel, C., 2014. Inventorying slope movements in an alpine environment using DInSAR. Earth Surf. Process. Landf. 39 (15), 2087–2099. http://dx.doi.org/10.1002/esp.3603.

Barrow, D.H., Tenenbaum, J.M., Bolles, R.C., Wolf, H.C., 1977. Parametric correspondence and chamfer matching: two new techniques for image matching. Proc. 5th Int. Joint Conf. Artificial Intelligence. Cambridge, MA, pp. 659–663.

Barsch, D., 1977. Nature and importance of mass-wasting by rock glaciers in alpine permafrost environment. Earth Surf. Process. Landf. 2 (2–3), 231–245. http://dx.doi.org/10.1002/esp.3290020213.

Bauer, A., Paar, G., Kaufmann, V., 2003. Permafrost. Ch. Terrestrial Laser Scanning for Rock Glacier Monitoring. Taylor and Francis, London, pp. 55–60.

Bodin, X., Schoeneich, P., 2008. High-resolution DEM extraction from terrestrial LIDAR topometry and surface kinematics of the creeping alpine permafrost: the Laurichard rock glacier case study (Southern French Alps). Proceedings of the Ninth International Conference on Permafrost.

Brodu, N., Lague, D., 2012. 3D terrestrial lidar data classification of complex natural scenes using a multi-scale dimensionality criterion: applications in geomorphology. ISPRS J. Photogramm. Remote Sens. 68, 121–134. http://dx.doi.org/10.1016/j.isprsjprs.2012.01.006.

Campello, R.J.G.B., Moulavi, D., Sander, J., 2013. Density-based clustering based on hierarchival density estimates. Proceedings of the 17th Pacific-Asia Conference on Knowledge Discovery in Databases, PAKDD 2013.

Chaplot, V., Bernoux, M., Walter, C., Curmi, P., Herpin, U., 2001. Soil carbon storage prediction in temperate hydromorphic soils using a morphologic index and digital elevation model. Soil Sci. 166 (1), 48–60. http://dx.doi.org/10.1097/00010694-200101000-00008.

Deems, J., Painter, T., Finnegan, D., 2013. LiDAR measurement of snow depth: a review. J. Glaciol. 59 (215), 467–479. http://dx.doi.org/10.3189/2013JoG12J154.

Delaloye, R., Lambiel, C., Gärtner-Roer, I., 2010. Overview of rock glacier kinematics research in the Swiss Alps. Seasonal rhythm, interannual variations and trends over several decades. Geog. Helv. 65, 135–145. http://dx.doi.org/10.5194/gh-65-135-2010.

EDF R&D, 2012. Cloudcompare (version 2.4) [gpl software]. . Tech. Rep.Telecom ParisTech.,

Ester, M., Kriegel, H.-P., Sander, J., Xu, X., 1996. A density-based algorithm for discovering clusters in large spatial databases with noise. Proc. 2nd Int. Conf. on Knowledge Discovery and Data Mining. AAAI Press, Portland, OR, pp. 226–231.

Fischer, M., Huss, M., Kummert, M., Hoelzle, M., 2016. Use of an ultra-long-range terrestrial laser scanner to monitor the mass balance of very small glaciers in the Swiss Alps. Cryosphere Discuss. http://dx.doi.org/10.5194/tc-2016-46. In review.

Florinsky, I.V., Kuryakova, G.A., 2000. Determination of grid size for digital terrain modeling in landscape investigations-exemplified by soil moisture distribution at a micro-scale. Int. J. Geogr. Inf. Sci. 14 (8), 815–832. http://dx.doi.org/10.1080/136588100750022804.

Gabbud, C., Micheletti, N., Lane, S.N., 2015. Lidar measurement of surface melt for a temperate alpine glacier at the seasonal and hourly scale. J. Glaciol. 61 (229), 963–974. http://dx.doi.org/10.3189/2015JoG14J226.

Gärtner-Roer, I., 2012. Sediment transfer rates of two active rock glaciers in the Swiss Alps. Geomorphology 167–168, 45–50. http://dx.doi.org/10.1016/j.geomorph.2012.04.013.

Gessler, P.E., Chadwick, O.A., Chamran, F., Althouse, L.D., Holmes, K.W., 2000. Modeling soil-landscape and ecosystem properties using terrain attributes. Soil Sci. Soc. Am. J. 64 (6), 2046–2056. http://dx.doi.org/10.2136/sssaj2000.6462046x.

Gigli, G., Casagli, N., 2011. Semi-automatic extraction of rock mass structural data from high resolution LIDAR point clouds. Int. J. Rock Mech. Min. Sci. 48 (2), 187–198. http://dx.doi.org/10.1016/j.ijrmms.2010.11.009.

Glenn, N.F., Streutker, D.R., Chadwick, D.J., Thackray, G.D., Dorsch, S.J., 2006. Analysis of LiDAR-derived topographic information for characterizing and differentiating landslide morphology and activity. Geomorphology 73 (1–2), 131–148. http://dx.doi.org/10.1016/j.geomorph.2005.07.006.

Hahsler, M., Piekenbrock, M., Arya, S., Mount, D., 2016. Density Based Clustering of Applications with Noise (DBSCAN) and Related Algorithms. Tech. Rep.. Package dbscan for R. https://cran.r-project.org/web/packages/dbscan/.

Harris, C., Arenson, L.U., et al. 2009. Permafrost and climate in Europe: monitoring and modelling thermal, geomorphological and geotechnical responses. Earth-Sci. Rev. 92 (3–4), 117–171. http://dx.doi.org/10.1016/j.earscirev.2008.12.002.

Heritage, G., Hetherington, D., 2007. Towards a protocol for laser scanning in fluvial geomorphology. Earth Surf. Process. Landf. 32 (1), 66–74. http://dx.doi.org/10.1002/esp.1375.

Jaboyedoff, M., Oppikofer, T., Abellan, A., Derron, M.-H., Loye, A., Metzger, R., Pedrazzini, A., 2012. Use of LIDAR in landslide investigations: a review. Nat. Hazards 61, 5–28. http://dx.doi.org/10.1007/s11069-010-9634-2.

Kääb, A., Frauenfelder, R., Roer, I., 2007. On the response of rockglacier creep to surface temperature increase. Glob. Planet. Chang. 56, 172–187. http://dx.doi.org/10.1016/j.gloplacha.2006.07.005.

Kellerer-Pirklbauer, A., Kaufmann, V., 2012. About the relationship between rock glacier velocity and climate parameters in Central Austria. Austrian Journal of Earth Sciences 105 (2), 94–112.

Lambiel, C., Delaloye, R., Strozzi, T., Lugon, R., Raetzo, H., 2008. ERS InSAR for assessing rock glacier activity. Proceedings of the Ninth International Conference on Permafrost.

Lambiel, C., Reynard, E., 2001. Regional modelling of present, past and future potential distribution of discontinuous permafrost based on a rock glacier inventory in the Bagnes-Hérémence area (Western Swiss Alps). Nor. J. Geol. 55 (4), 219–223. http://dx.doi.org/10.1080/00291950152746559.

Lane, S.N., Chandler, J.H., Richards, K.S., 1994. Developments in monitoring and modelling small-scale river bed topography. Earth Surf. Process. Landf. 19 (4), 349–368. http://dx.doi.org/10.1002/esp.3290190406.

Lane, S.N., Westaway, R.M., Murray Hicks, D., 2003. Estimation of erosion and deposition volumes in a large, gravel-bed, braided river using synoptic remote sensing. Earth Surf. Process. Landf. 28 (3), 249–271. http://dx.doi.org/10.1002/esp.483.

Lugon, R., Stoffel, M., 2010. Rock-glacier dynamics and magnitude-frequency relations of debris flows in a high-elevation watershed: Ritigraben, Swiss Alps. Glob. Planet. Chang. 73, 202–210. http://dx.doi.org/10.1016/j.gloplacha.2010.06.004.

MeteoSwiss, 2016. Climatic report, year 2015. . Tech. Rep., Zürich http://www.meteoswiss.admin.ch/home/climate/present-day/climate-reports.html.

Micheletti, N., Lambiel, C., Lane, S.N., 2015. Investigating decadal-scale geomorphic dynamics in an alpine mountain setting. J. Geophys. Res. Earth Surf. 120, 2155–2175. http://dx.doi.org/10.1002/2015jf003656.

Neugirg, F., Stark, M., Kaiser, A., Vlacilova, M., Della Seta, M., Vergari, F., Schmidt, J., Becht, M., Haas, F., 2016. Erosion processes in Calanchi in the Upper Orcia Valley, Southern Tuscany, Italy based on multitemporal high-resolution terrestrial LiDAR and UAV surveys. Geomorphology 269, 8–22. http://dx.doi.org/10.1016/j.geomorph.2016.06.027.

Olsen, M.J., Wartman, J., McAlister, M., Mahmoudabadi, H., O'Banion, M.S., Dunham, L., Cunningham, K., 2015. To fill or not to fill: sensitivity analysis of the influence of resolution and hole filling on point cloud surface modeling and individual rockfall event detection. Remote Sens. 7, 12103–12134. http://dx.doi.org/10.3390/rs70912103.

Core Team, R., 2015. R: A Language and Environment for Statistical Computing. R Foundation for Statistical Computing, Vienna, Austria. https://www.R-project.org.

Riquelme, A.J., Abellan, A., Tomas, M., Jaboyedoff, M., 2014. A new approach for semi-automatic rock mass joints recognition from 3D point clouds. Comput. Geosci. 68, 38–52. http://dx.doi.org/10.1016/j.cageo.2014.03.014.

Rohmer, J., Dewez, T., 2015. Analysing the spatial patterns of erosion scars using point process theory at the coastal chalk cliff of Mesnil-Val, Normandy, northern France. Nat. Hazards Earth Syst. Sci. 15, 349–362. http://dx.doi.org/10.5194/nhess-15-349-2015.

Schaefer, M., Inkpen, R., 2010. Towards a protocol for laser scanning of rock surfaces. Earth Surf. Process. Landf. 35 (4), 417–423. http://dx.doi.org/10.1002/esp.1938.

Tonini, M., Abellan, A., 2014. Rockfall detection from terrestrial LiDAR point clouds: a clustering approach using R. J. Spat. Inf. Sci. 8, 95–110. http://dx.doi.org/10.5311/josis.2014.8.123.

Zhang, Z., 1994. Iterative point matching for registration of free-form curves. Int. J. Comput. Vis. 13, 119–152. http://dx.doi.org/10.1007/bf01427149.